IMECE'02
2002 ASME INTERNATIONAL MECHANICAL ENGINEERING CONGRESS AND EXPOSITION
November 17–22, 2002, New Orleans, Louisiana

IMECE2002-33979

MICRO-CONTROL ACTIONS OF SEGMENTED ACTUATORS ON SHALLOW PARABOLOIDAL SHELL REFLECTORS

S.-S. Lih [1], G. Hickey [1], J. H. Ding [2], and H. S. Tzou [2]

[1] Jet Propulsion Laboratory,
California Institute of Technology,
Pasadena, CA 91109

[2] Department of Mechanical Engineering,
StrucTronics Lab, University of Kentucky,
Lexington, KY 40506

ABSTRACT

Shallow paraboloidal shells of revolution are common components for reflectors, mirrors, etc. This study is to investigate the micro-control actions and distributed control effectiveness of precision paraboloidal shell structures laminated with segmented actuator patches. Mathematical models and governing equations of the paraboloidal shells laminated with distributed actuator layers segmented into patches are presented first, followed by formulations of distributed control forces and micro-control actions including meridional/circumferential membrane and bending control components based on an assumed mode shape function and the Taylor series expansion. Distributed control forces, patch sizes, actuator locations, micro-control actions, and normalized control authorities of a shallow paraboloidal shell are then analyzed in a case study. Analysis indicates that 1) the control forces and membrane/bending components are mode and location dependent, 2) the meridional/circumferential membrane control actions dominate the overall control effect, 3) there are optimal actuator locations resulting in the maximal control effects at the minimal control cost for each natural mode. The analytical results provide generic design guidelines for actuator placement on precision shallow paraboloidal shell structures.

INTRODUCTION

The space science community has identified a need for ultra-light weight spacecraft due to the reduction of launch mass and increasing stowage efficiency. The applications include solar sails, concentrators, radar, antenna, and large aperture optical systems.

Large optical aperture systems as well as other ultra-lightweight optical systems require deployable and precise thin structural surface (e.g. Ref. 1-4). Conventional lightweight deployable space structures often utilize kinematic mechanisms driven by motors in the deployment process such as Next Generation Space telescope (NGST). In general, these mechanisms are bulky, complicated, and nee sophisticated operational process. Advanced deployable mechanisms are required to provide a much more efficient large spacecraft.

Current mirror technologies are limiting due either to high areal density of the optical substrates or supporting structure, or to poor dimensional stability in a space environment. For space-based systems, the limiting geometric factor for monolithic deployed structures is the diameter of the launch vehicle shroud. To over come this, several people have proposed membrane optics. For these systems, one of the most rigorous requirements in the design of astronomical optical membrane is the maintenance of the primary optical aperture surface figure to very high degree of accuracy. Typical optical membranes range in thickness from 10-150 micrometers, with maximum acceptable peak-to-peak figure errors in the range from 10-20 micrometers. The shape of the optical membrane has to be continuously monitored for these wavelengths, and any deviation from the desired shape caused by external disturbances needs to be controlled or compensated for in secondary optics or image reconstruction. It is therefore desirable to have Precision Ultra-lightweight Apertures (PUA) for practical applications such as imaging and communications. An adaptive membrane system that can be used to accurately control the shape of a deformable optical aperture is among one of the best viable selections.

In general, adaptive mirrors and reflectors with discrete drivers are widely used for compensating the wavefront distortions by activating the drives at definite positions. The mirror systems with discrete drivers almost always include a large quantity of actuators that cause tremendous efforts in the manufacturing and controlling process and the high numbers of actuators and cabling dominate the mass. In contrast to discrete actuating mechanisms the distributed active systems are constructed by embedding or bonding active materials continuously over the whole mirror structure. The deformation mechanism of a distributed actuation system is less rigid than that composed of discrete drivers. It can be seen that the deployment and performance are two key factors that dominate the success and user acceptance of the large precision apertures. Thus, one can see that the controllable adaptive thin deployable low-mass membrane structures are essential for these future applications. Through the development and advancement of lightweight, high performance active materials such as piezoelectric, electrostrictive, shape memory materials in the past few years and through the progress of the microelectronic control technology, the industries begin to be aware of the application of these materials as actuators for the adaptive aperture structures. The applications of electroactive materials as actuators for the deformable membrane apertures become more promising and practical.

To achieve the goal of the shape control of an adaptive precision membrane structure, the authors studied the micro-control actions and distributed control effectiveness of precision paraboloidal shell structures laminated with segmented actuator patches in this paper. In this study, mathematical models of the paraboloidal shells laminated with distributed actuator layers segmented into patches are defined first, followed by formulations of distributed control forces and detailed membrane/bending micro-control actions. Distributed actuator control forces and control authorities at various actuator locations on a shallow paraboloidal shell reflector are investigated. Distributed modal control effects and micro-meridional/circumferential membrane/bending control actions are evaluated and general design guidelines are proposed. Put introduction here.

NOMENCLATURE

Put nomenclature here.

MODELING AND DISTRIBUTED ACTUATION

A generic shallow paraboloidal shell of revolution is defined in a tri-orthogonal coordinate system, **Figure 1**, where $\alpha_1 = \phi$ denotes the meridional axis, $\alpha_2 = \psi$ denotes the circumferential axis, a meridional radius of curvature $R_1 = R_\phi = b/\cos^3\phi$, a circumferential radius of curvature $R_2 = R_\psi = b/\cos\phi$, and the constant $b = a^2/(2c) = 2f$ where "a" is the radial distance, "c" is the meridian height at the pole, and "f" is the focal length. The Lamé parameters of a paraboloidal shell are $A_1 = b/(\cos^3\phi)$ and $A_2 = (b\sin\phi)/(\cos\phi)$. Mathematical models are defined first, followed by micro-control actions and their control effectiveness of segmented actuator patches in this section.

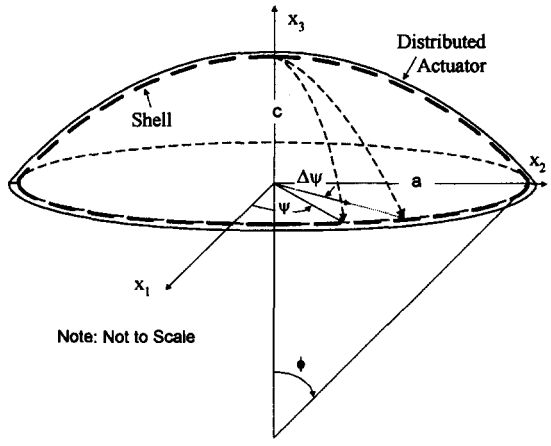

Figure 1. A shallow paraboloidal shell laminated with a distributed actuator layer.

Mathematical model of paraboloidal shell reflectors with spatially distributed actuator induced control actions can be defined. Three coupled elastic/control governing equations respectively in the meridional, the circumferential, and the transverse directions are

$$\frac{1}{\cos^3\phi}\frac{\partial}{\partial\psi}(N^m_{\psi\phi}) + \frac{\partial}{\partial\phi}[(N^m_{\phi\phi} - N^a_{\phi\phi})\tan\phi] - (N^m_{\psi\psi} - N^a_{\psi\psi})\frac{1}{\cos^2\phi} + Q_{\phi 3}\tan\phi + \frac{b\sin\phi}{\cos^4\phi}q_\phi = \frac{b\sin\phi}{\cos^4\phi}\rho h\frac{\partial^2 u_\phi}{\partial t^2} \tag{1}$$

$$\frac{1}{\cos^3\phi}\frac{\partial}{\partial\psi}(N^m_{\psi\psi} - N^a_{\psi\psi}) + \frac{\partial}{\partial\phi}(N^m_{\phi\psi}\tan\phi) + N^m_{\psi\phi}\frac{1}{\cos^2\phi} + \frac{\sin\phi}{\cos^3\phi}Q_{\psi 3} + \frac{b\sin\phi}{\cos^4\phi}q_\psi = \frac{b\sin\phi}{\cos^4\phi}\rho h\frac{\partial^2 u_\psi}{\partial t^2} \tag{2}$$

$$\frac{\cos\phi}{b\sin\phi}\frac{\partial}{\partial\psi}[\sec^3\phi\frac{\partial}{\partial\psi}(M^m_{\psi\psi} - M^a_{\psi\psi}) + \frac{\partial}{\partial\phi}(M^m_{\psi\phi}\tan\phi) + M^m_{\psi\phi}\sec^2\phi] + \frac{1}{b}\frac{\partial}{\partial\phi}\{\frac{\partial}{\partial\psi}M^m_{\psi\phi} + \cos^3\phi\frac{\partial}{\partial\phi}[(M^m_{\phi\phi} - M^a_{\phi\phi})\tan\phi] - (M_{\psi\psi} - M^a_{\psi\psi})\cos\phi\}$$
$$- (N^m_{\phi\phi} - N^a_{\phi\phi})\tan\phi - (N^m_{\psi\psi} - N^a_{\psi\psi})\frac{\sin\phi}{\cos^3\phi} + q_3\frac{b\sin\phi}{\cos^4\phi} = \frac{b\sin\phi}{\cos^4\phi}\rho h\frac{\partial^2 u_3}{\partial t^2} \tag{3}$$

where ρ is the mass density; h is the shell thickness; q_i is the input force; $Q_{\phi 3}$ and $Q_{\psi 3}$ are the transverse shear effects; and the superscripts "m" and "a" respectively denote the elastic (or mechanical) and electrically induced control actions. N^m_{ij} and M^m_{ij} are the elastic forces and moments; N^a_{ij} and M^a_{ij} are the electric control forces and moments, respectively. The elastic force and moment resultants of thin paraboloidal shells following the Love-Kirchoff thin shell assumptions are defined as

$$N^m_{\phi\phi} = \frac{K}{b}[\cos^3\phi\frac{\partial u_\phi}{\partial\phi} + \mu\cot\phi\frac{\partial u_\psi}{\partial\psi} + \mu\frac{\cos^2\phi}{\sin\phi}u_\phi + (\cos^3\phi + \mu\cos\phi)u_3] \tag{4}$$

$$N^m_{\psi\psi} = \frac{K}{b}[\cot\phi\frac{\partial u_\psi}{\partial\psi} + \frac{\cos^2\phi}{\sin\phi}u_\phi + \mu\cos^3\phi\frac{\partial u_\phi}{\partial\phi} + (\cos\phi + \mu\cos^3\phi)u_3] \quad (5)$$

$$N^m_{\phi\psi} = \frac{K(1-\mu)}{2b}[-\frac{\cos^2\phi}{\sin\phi}u_\psi + \cos^3\phi\frac{\partial u_\psi}{\partial\phi} + \frac{\cos\phi}{\sin\phi}\frac{\partial u_\phi}{\partial\psi}] \quad (6)$$

$$M^m_{\phi\phi} = \frac{D}{b^2}\{\cos^6\phi(\frac{\partial u_\phi}{\partial\phi} - \frac{\partial^2 u_3}{\partial\phi^2}) - 3\cos^5\phi\sin\phi(u_\phi - \frac{\partial u_3}{\partial\phi}) + \mu\frac{\cos^2\phi}{\sin\phi}(\frac{\partial u_\psi}{\partial\psi} - \frac{1}{\sin\phi}\frac{\partial^2 u_3}{\partial\psi^2} + u_\phi\cos^3\phi - \cos^3\phi\frac{\partial u_3}{\partial\phi})\} \quad (7)$$

$$M^m_{\psi\psi} = \frac{D}{b^2}\{\frac{\cos^2\phi}{\sin\phi}(\frac{\partial u_\psi}{\partial\psi} - \frac{1}{\sin\phi}\frac{\partial^2 u_3}{\partial\psi^2} + u_\phi\cos^3\phi - \cos^3\phi\frac{\partial u_3}{\partial\phi}) + \mu[\cos^6\phi(\frac{\partial u_\phi}{\partial\phi} - \frac{\partial^2 u_3}{\partial\phi^2}) - 3\cos^5\phi\sin\phi(u_\phi - \frac{\partial u_3}{\partial\phi})]\} \quad (8)$$

$$M^m_{\phi\psi} = \frac{D(1-\mu)}{2}(-\frac{\cos^5\phi + 2\cos^3\phi\sin^2\phi}{b^2\sin\phi}u_\psi + \frac{2\cos^3\phi}{b^2\sin^2\phi}\frac{\partial u_3}{\partial\psi} - \frac{2\cos^4\phi}{b^2\sin\phi}\frac{\partial^2 u_3}{\partial\psi\partial\phi} + \frac{\cos^4\phi}{b^2}\frac{\partial u_\psi}{\partial\phi} + \frac{\cos^4\phi}{b^2\sin\phi}\frac{\partial u_\phi}{\partial\psi}) \quad (9)$$

The membrane stiffness $K = Yh/(1-\mu^2)$ and the bending stiffness $D = Yh^3/[12(1-\mu^2)]$, where Y is the modulus of elasticity and μ is Poisson's ratio of the shell. Furthermore, the distributed actuator layer is segmented into actuator patches on the shallow paraboloidal shell reflector as in **Figure 2**. Control forces and micro-control actions of actuator patches at various locations are evaluated.

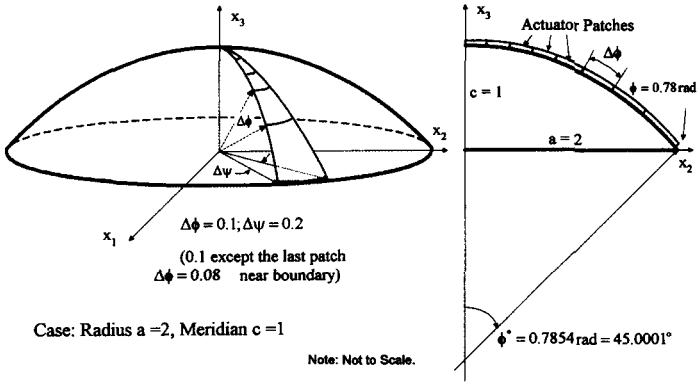

Figure 2. A shallow paraboloidal shell reflector laminated with segmented distributed actuator patches.

The control forces/moments induced by the applied control signal ϕ^a in the spatially distributed piezoelectric actuator layer are (Tzou, 1993)

$$N^a_{\phi\phi} = d_{31}Y_p\phi^a \quad (10)$$

$$N^a_{\psi\psi} = d_{32}Y_p\phi^a \quad (11)$$

$$M^a_{\phi\phi} = r^a_\phi d_{31}Y_p\phi^a \quad (12)$$

$$M^a_{\psi\psi} = r^a_\psi d_{32}Y_p\phi^a \quad (13)$$

where ϕ^a (in *italic*) is the control signal; Y_p is Young's modulus of the distributed actuator; d_{3i} are the piezoelectric strain constants; r^a_i denote the location (the moment arm) measured from the shell neutral surface to the mid-plane of the distributed actuator. Also, the transverse control signal $\phi^a(\phi,\psi,t)$ is only confined on the segmented actuator patch electrode ranging from ϕ_1 to ϕ_2 and from ψ_1 to ψ_2.

$$\phi^a(\phi,\psi,t) = \phi^a(t)[u_s(\phi-\phi_1) - u_s(\phi-\phi_2)][u_s(\psi-\psi_1) - u_s(\psi-\psi_2)] \quad (14)$$

where $u_s(\cdot)$ is the unit step function: $u_s(\phi-\phi_i) = 1$ when $\phi > \phi_i$, and = 0 when $\phi < \phi_i$. For uniform-thickness actuator and shell, $r^a_\phi = r^a_\psi$. Since the electric resistance on the actuator surface is negligible, the electric potential on the actuator surface is assumed constant and separated by patch divisions. For conventional hexagonal piezoelectric actuator patches, the in-plane twisting (shear) effects are usually neglected, i.e., $N^a_{\phi\psi} \approx 0$ and $M^a_{\phi\psi} \approx 0$. Also, the actuator layer is thin and its mass and stiffness properties can be neglected. Thus, only the control actions are considered. Considering the resultant elastic and control effects, one can re-define the total force/moment resultants, including the elastic components and the control forces/moments induced by actuator patches.

$$N_{\phi\phi} = \frac{K}{b}[\cos^3\phi\frac{\partial u_\phi}{\partial\phi} + \mu\cot\phi\frac{\partial u_\psi}{\partial\psi} + \mu\frac{\cos^2\phi}{\sin\phi}u_\phi + (\cos^3\phi + \mu\cos\phi)u_3] - d_{31}Y_p\phi^a \quad (15)$$

$$N_{\psi\psi} = \frac{K}{b}[\cot\phi\frac{\partial u_\psi}{\partial\psi} + \frac{\cos^2\phi}{\sin\phi}u_\phi + \mu\cos^3\phi\frac{\partial u_\phi}{\partial\phi} + (\cos\phi + \mu\cos^3\phi)u_3] - d_{32}Y_p\phi^a \quad (16)$$

$$M_{\phi\phi} = \frac{D}{b^2}\{\cos^6\phi(\frac{\partial u_\phi}{\partial\phi} - \frac{\partial^2 u_3}{\partial\phi^2}) - 3\cos^5\phi\sin\phi(u_\phi - \frac{\partial u_3}{\partial\phi}) + \mu\frac{\cos^2\phi}{\sin\phi}(\frac{\partial u_\psi}{\partial\psi} - \frac{1}{\sin\phi}\frac{\partial^2 u_3}{\partial\psi^2} + u_\phi\cos^3\phi - \cos^3\phi\frac{\partial u_3}{\partial\phi})\} - r^a_\phi d_{31}Y_p\phi^a \quad (17)$$

$$M_{\psi\psi} = \frac{D}{b^2}\{\frac{\cos^2\phi}{\sin\phi}(\frac{\partial u_\psi}{\partial\psi} - \frac{1}{\sin\phi}\frac{\partial^2 u_3}{\partial\psi^2} + u_\phi\cos^3\phi - \cos^3\phi\frac{\partial u_3}{\partial\phi}) + \mu[\cos^6\phi(\frac{\partial u_\phi}{\partial\phi} - \frac{\partial^2 u_3}{\partial\phi^2}) - 3\cos^5\phi\sin\phi(u_\phi - \frac{\partial u_3}{\partial\phi})]\} - r^a_\psi d_{32}Y_p\phi^a. \quad (18)$$

Due the complexity of analytical solution procedures of the coupled elastic/electromechanical/control equations, evaluation of distributed micro-control effects is based on an assumed solution satisfying the given boundary conditions, although the closed-form system equations of paraboloidal shells are defined.

DISTRIBUTED MICRO-CONTROL ACTIONS

Based on the modal expansion method, the total shell response is composed of all participating modes, i.e., $u_i(\alpha_1,\alpha_2,t) = \sum_{m=1}^{\infty}\eta_m(t)U_{im}(\alpha_1,\alpha_2)$ where $\eta_m(t)$ is the m-th modal participating factor or the m-th modal coordinate

and $U_{im}(\alpha_1,\alpha_2)$ is the mode shape function. Accordingly, the original distributed control equation can be transferred into the modal domain and individual modal control equations can be evaluated based on the mode shape functions and the distributed actuator patch defined from ϕ_1 to ϕ_2 and from ψ_1 to ψ_2. The displacement and the moment on the boundary perimeter are assumed zero for a simply supported parabolodial shell structure. Also, since the transverse axisymmetric oscillation dominates, the transverse mode shape function U_{3m} can be approximated by

$$U_{3m} = A_m \cos\frac{(2m-1)\pi}{2\phi^*}\phi = A_m \cos B_m\phi, m = 1,2,...,\infty \quad (19)$$

where A_m is the mth modal amplitude, $B_m = [(2m-1)\pi]/(2\phi^*)$, ϕ is the meridional angle measured from the pole ($\phi = 0$) to the shell boundary rim at $\phi = \phi^*$. Accordingly, the modal control equation becomes

$$\ddot{\eta}_m + \frac{c}{\rho h}\dot{\eta}_m + \omega_m^2\eta_m = \hat{F}_m \quad (20)$$

where c is the damping constant; ω_m is the m-th natural frequency; and $\hat{F}_m$ is the distributed modal control force. Imposing the axisymmetric assumption, i.e., $\partial(\bullet)/\partial\psi = 0$, assuming the uniform-thickness actuator and shell, i.e., $r_\phi^a = r_\psi^a = r^a$, the hexagonal piezoelectric materials, i.e., $d_{31} = d_{32}$, and substituting the control forces/moments, one can define the modal control force induced by the segmented distributed actuator defined by ϕ_1 to ϕ_2 and ψ_1 to ψ_2.

$$\begin{aligned}\hat{F}_m = {} & \frac{Y_p d_{31} A_m \phi^a(t)}{\rho h N_m} \\ & \cdot\int_{\phi_1}^{\phi_2}\int_{\psi_1}^{\psi_2}\{ r^a\{-\cos^5\phi[u_s(\psi-\psi_1)-u_s(\psi-\psi_2)]\frac{\partial}{\partial\phi}[\delta(\phi-\phi_1)-\delta(\phi-\phi_2)] \\ & + \frac{\cos^4\phi(3\sin^2\phi-2)}{\sin\phi}[\delta(\phi-\phi_1)-\delta(\phi-\phi_2)][u_s(\psi-\psi_1)-u_s(\psi-\psi_2)] \\ & + \frac{\cos^4\phi}{\sin\phi}[\delta(\phi-\phi_1)-\delta(\phi-\phi_2)][u_s(\psi-\psi_1)-u_s(\psi-\psi_2)]\} \\ & + b\cos^2\phi[u_s(\phi-\phi_1)-u_s(\phi-\phi_2)][u_s(\psi-\psi_1)-u_s(\psi-\psi_2)] \\ & + b[u_s(\phi-\phi_1)-u_s(\phi-\phi_2)][u_s(\psi-\psi_1)-u_s(\psi-\psi_2)]\} \\ & \frac{\cos B_m\phi\sin\phi}{\cos^3\phi}d\phi d\psi\end{aligned} \quad (21)$$

where

$$N_m = \int_\psi\int_\phi U_{3m}^2 A_1 A_2 d\phi d\psi = \psi^* A_m^2 b^2\int_0^{\phi^*}\cos^2 B_m\phi\frac{\sin\phi}{\cos^4\phi}d\phi$$

ψ^* is the circumferential boundary angle and $\psi^* = 2\pi$ for a circumferentially closed shell, $\delta(\cdot)$ is the Dirac delta function, and $u_s(\cdot)$ is the unit step function. Analytical solution of N_m is carried out using the Taylor series expansion and the surface integration defined by the distributed actuator is carried out to evaluate the patch modal control force. Furthermore, the detailed micro-control action can be divided into its contributing microscopic meridional/circumferential bending and membrane control actions.

$$\begin{aligned}\hat{F}_m &= \frac{Y_p d_{31} A_m \phi^a(t)}{\rho}[(\hat{T}_m)_{Total}] \\ &= \frac{Y_p d_{31} A_m \phi^a(t)}{\rho}[(\hat{T}_m)_{\phi,bend} + (\hat{T}_m)_{\psi,bend} + (\hat{T}_m)_{\phi,mem} + (\hat{T}_m)_{\psi,mem}]\end{aligned} \quad (22)$$

where $(\hat{T}_m)_{Total}$ denotes the overall control effect, excluding the coefficients and modal parameters; $(\hat{T}_m)_{\phi,bend}$, $(\hat{T}_m)_{\psi,bend}$, $(\hat{T}_m)_{\phi,mem}$ and $(\hat{T}_m)_{\psi,mem}$ respectively denote the control effect resulting from $M_{\phi\phi}^c$ - the control moment in the ϕ direction, $M_{\psi\psi}^c$ - the control moment in the ψ direction, $N_{\phi\phi}^c$ - the control force in the ϕ direction, and $N_{\psi\psi}^c$ - the control force in the ψ direction. These individual contributing control effects are evaluated in case studies. Note that surface integrations in the modal force expression are difficult to carry out exactly. Again, the Taylor series expansion technique is used in the solution procedures.

CASE STUDY

The aberrations for different mirror structures are varied in a wide range. Table I shows a typical PV range of Seidel aberrations for a 100mm aperture mirror, where r is radius, $\psi 0$ is the reference angle, AD, AS, AG, and AC are the amplitude parameters for defocusing, spherical aberration, astigmatism, and coma, respectively.

Table I. The PV range of Seidel aberrations for a 100mm aperture mirror.igure 2. A shallow paraboloidal shell reflector laminated with segmented distributed actuator patches.

Aberration	Representation	PV, micron
Defocusing	$A_D r^2$	10.8
Spherical aberration	$A_S r^4$	3.5
Astigmatism	$A_G r^2\cos(\psi+\psi_0)$	0.55
Coma	$A_C r^2\cos(\psi+\psi_0)$	0.47

As shown in Table I, these and other kinds of aberration need to be corrected through an optimal design of the arrangement of actuators and a practical control mechanism. To achieve this, distributed control effects, micro-contributing control actions,

effective actuator sizes, and normalized control authorities of a simply-supported shallow paraboloidal shell reflector (with the meridional angle $\phi^* = 0.7854$ radians, the meridian/radius ratio = ½, thickness h=0.002) laminated with segmented actuator patches are first studied, **Figure 2.** The actuator patch size is $\Delta\phi = \phi_2 - \phi_1 = 0.1$ radians defined in the meridional direction and a "circumferential width" $\Delta\psi = \psi_2 - \psi_1 = 0.2$ radians. Note that these patch sizes (or the projected meridional and circumferential arc lengths) are not identical as they move from the pole to the rim, because of the curvature effect. Actuator induced forces, micro-control actions, and control effectiveness of the "standard" actuator patch ($\Delta\phi$ = 0.1; $\Delta\psi$ = 0.2) located at various locations are evaluated in section. Recall that $(\hat{T}_m)_{Total}$ denotes the total control force, $(\hat{T}_m)_{\psi,mem}$ the circumferential membrane micro-control action, $(\hat{T}_m)_{\phi,mem}$ the meridional membrane micro-control action, $(\hat{T}_m)_{\phi,bend}$ the meridional bending micro-control action, $(\hat{T}_m)_{\psi,bend}$ the circumferential bending micro-control action. Modal control force and micro-control actions, i.e., $(\hat{T}_m)_{Total}$, $(\hat{T}_m)_{\phi,bend}$, $(\hat{T}_m)_{\psi,bend}$, $(\hat{T}_m)_{\phi,mem}$, and $(\hat{T}_m)_{\psi,mem}$ for the first three modes are calculated and plotted in **Figures 3-5.** Note that the vertical axis is the force magnitude and the horizontal axis is the projected diameter of the shallow paraboloidal shell. They show the variation of control forces along the shell surface in the meridional direction. (Note that T_m denotes $\hat{T}_m$ in these figures). Accordingly, each data point represents the actuator's micro-control effects at a specific patch location moving from the top pole to the bottom rim in the meridional direction.

The resultant control effects of actuator patches depend on the patch locations and the mode shape variations; these forces are symmetric due to the axisymmetric assumption of the mode shape functions. Note that there are positive and negative control forces induced by the actuator patch moving in the meridional direction on the shell surface. The positive forces induce positive control effects and the negative forces aggravate the vibrations when the positive control signals are used. However, since the sign of control signals can be manipulated in the control circuit, one should look at the "absolute" magnitudes to infer the "absolute" control effectiveness at these locations. Detailed micro-control actions reveal that the circumferential and meridional membrane control forces dominate the overall control effects and the bending (both meridional and circumferential) control moments are relatively insignificant. These micro-control effects (meridional/circumferential membrane and bending control effects) are respectively calculated based on the modal force formulation including the effects of actuator sizes.

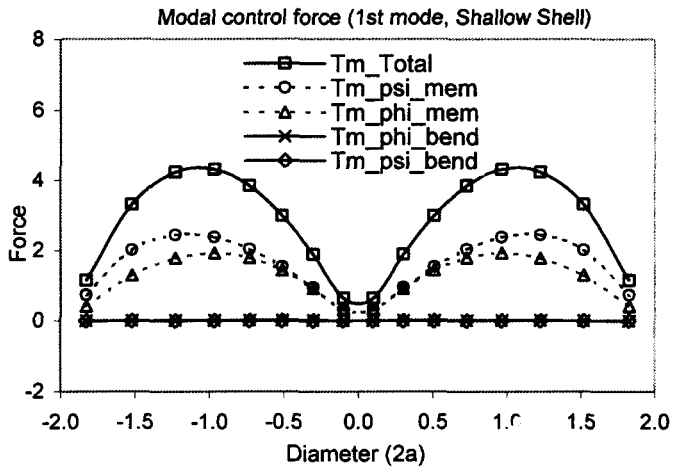

Figure 3. Modal control forces and micro-control actions at various actuator locations, 1st mode, $\Delta\phi$ = 0.1. (□: $(\hat{T}_m)_{Total}$, o: $(\hat{T}_m)_{\psi,mem}$, Δ: $(\hat{T}_m)_{\phi,mem}$, ×: $(\hat{T}_m)_{\phi,bend}$, ◊: $(\hat{T}_m)_{\psi,bend}$)

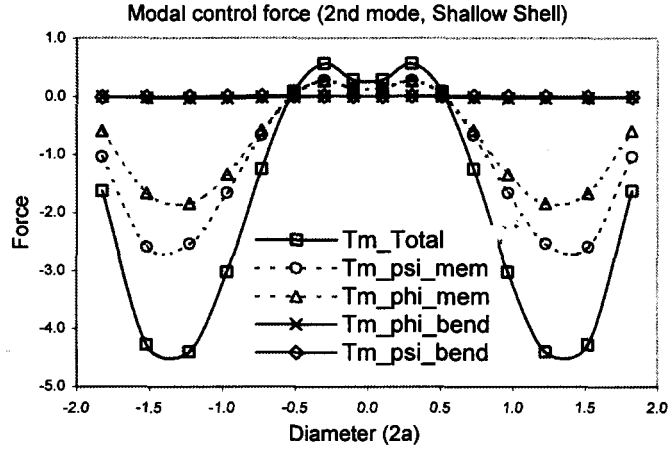

Figure.4 Modal control forces and micro-control actions at various actuator locations, 2nd mode, $\Delta\phi$ = 0.1.

Since these actuator sizes are not constant, these control forces and their micro-control effects need to be normalized in order to evaluate the true control effect per unit actuator area. Considering the curvature variations influencing the projected arc lengths, one can calculate the "true" actuator size at a given location on the deep paraboloidal shell. **Figure 6** indicates that the actuator size changes significantly, depending on the patch location of the shallow paraboloidal shell, although they keep identical $\Delta\phi = 0.1$ and $\Delta\psi = 0.2$ radians. Thus, the control forces and the micro-control actions are normalized with respect to the actuator size and these normalized meridional/circumferential membrane and bending components of the first three paraboloidal shell modes are presented in **Figures 7-9.**

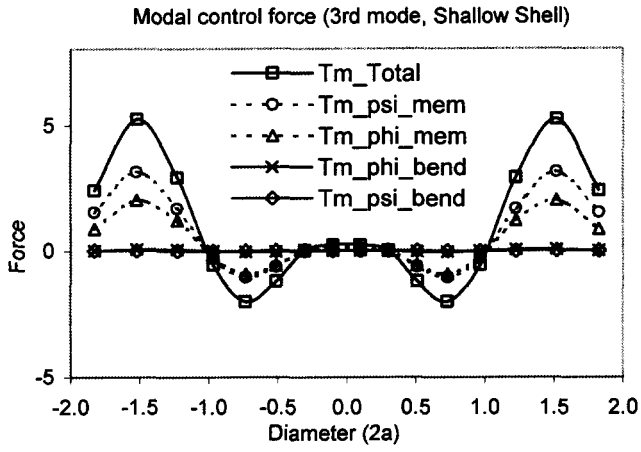

Figure 5. Modal control forces and micro-control actions at various actuator locations, 3rd mode, $\Delta\phi = 0.1$.

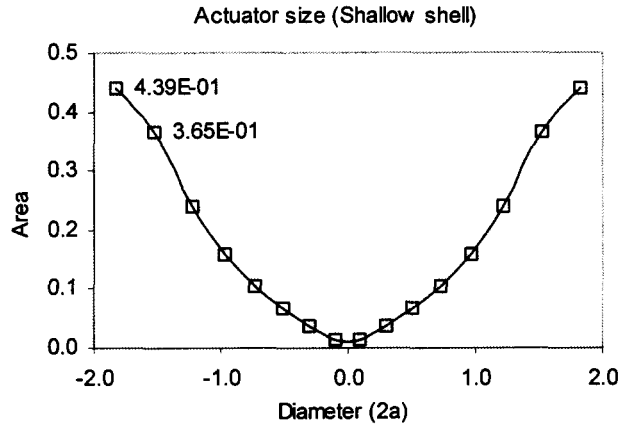

Figure 6. Effective actuator sizes at various patch locations, (shallow shells), $\Delta\phi = 0.1$.

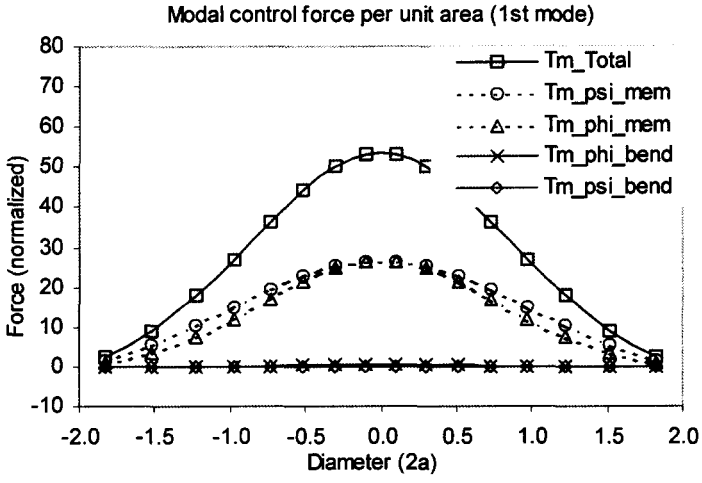

Figure 7. Normalized modal control forces and micro-control actions at various locations, 1st mode, $\Delta\phi = 0.1$.

(□: $(\hat{T}_m)_{Total}$, o: $(\hat{T}_m)_{\psi,mem}$, Δ: $(\hat{T}_m)_{\phi,mem}$, ×: $(\hat{T}_m)_{\phi,bend}$, ◊: $(\hat{T}_m)_{\psi,bend}$)

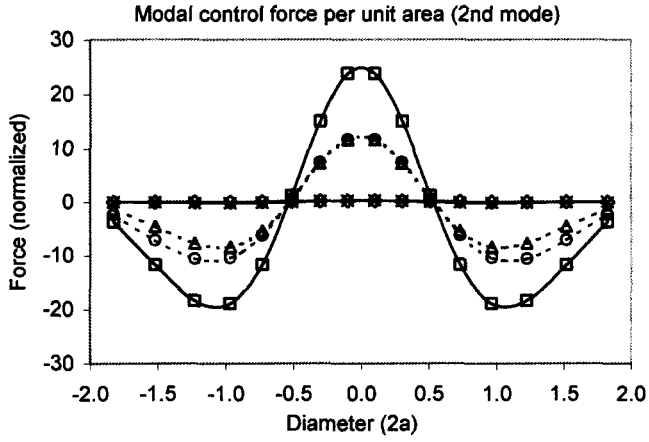

Figure 8. Normalized modal control forces and micro-control actions at various locations, 2nd mode, $\Delta\phi = 0.1$.

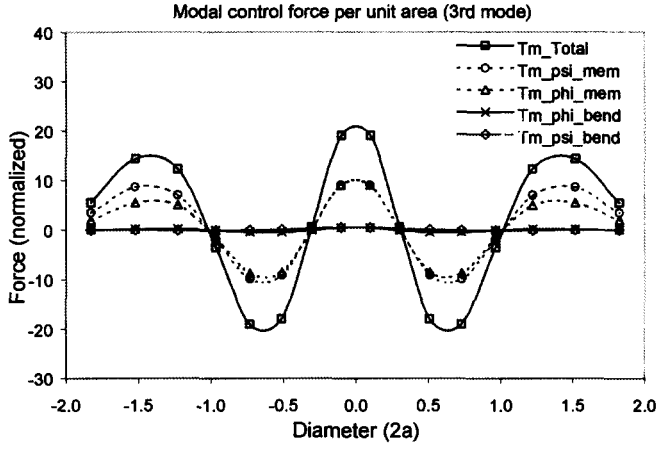

Figure 9. Normalized modal control forces and micro-control actions at various locations, 3rd mode, $\Delta\phi = 0.1$.

These normalized control actions of actuator patches show the variation of control forces per unit area along the shell meridional surface and the "size effect" is excluded. Higher nominal values imply that the induced control actions per unit area (or control authorities/actuator size) are higher, i.e., higher control effects at given control cost or power. These data indicate that actuator patches located at the pole provide the best control effects for the first mode. There are three effective locations for the second mode and five locations for the third mode. In any case, centrally located actuator patch yields the most effective control effect for most natural modes of the simply-supported shallow paraboloidal shell reflector.

CONCLUSIONS

The space science community has identified a need for ultra-light weight large deployed structures spacecraft due to the reduction of launch mass and increasing stowed efficiency. The applications include solar sails, concentrators, radar, antenna, and large aperture optical systems. Shallow paraboloidal shells are common components for varieties of high-precision aerospace structures. This study evaluated the control effectiveness of distributed segmented actuator patches and examined their microscopic control actions and authorities

of these actuator patches laminated on a thin shallow paraboloidal shell. Mathematical models of the paraboloidal shell and the distributed actuator patches were defined first, followed by governing system equations. Theoretical derivations of distributed control forces reveal that the micro-control actions of actuator patches can be divided into 1) the meridional membrane effect, 2) the circumferential membrane effect, 3) the meridional bending effect, and 4) the circumferential bending effect. These micro-control actions were analyzed in a case study. Analytical solutions based on the assumed mode shape function of a simply-supported (or knife-edge) shallow paraboloidal shell were derived.

Analysis of control forces and micro-control actions (control forces and control moments) suggests that these control actions are sensitive to actuator locations and natural modes; they generally decrease as the mode number increases. Among the four control actions, the meridional and circumferential membrane control force components dominate the overall control effect and the meridional control action is slightly higher than the circumferential control action. The bending control actions (both meridional and circumferential) are very small for lower shell modes and they gradually increase as the mode increases when the shell's bending behavior becomes observable. The bending control action is proportional to the shell thickness and it increases as the shell becomes thicker, while the membrane control action remains constant. Furthermore, analysis of micro-control actions, actuator locations, actuator-size variations related to mode shapes reveals a number of ideal patch locations introducing the maximal control effects at the minimal control cost or actuator size. These analysis data provide general design guidelines and optimal actuator locations for precision control of shallow paraboloidal shell structronic systems.

ACKNOWLEDGMENTS

This research was carried out at the Jet Propulsion Laboratory, California Institute of Technology, under a contract with the National Aeronautics and Space Administration and University of Kentucky. Reference herein to any specific commercial product, process, or service by trade name, trademark, manufacturer, or otherwise, does not constitute or imply its endorsement by the United States Government or the Jet Propulsion Laboratory, California Institute of Technology.

REFERENCES

1. Jenkins, C. H., Kalanovic, V.D. , Padmanabhan, K. and Faisal, S. M. , 1999, "Intelligent Shape Control for Precision Membrane Antennae and Reflectors in Space, ", *Smart Matls. Struct 8*, pp.1-11.
2. Robertson, H.J., Crane, R. and Hemstreet, H.S, Oct., 1966, "Active Optics System for Spaceborne Telescopes, " *NASA CR-66297.*
3. Kuo, C. P., 1994, "Optical Tests Of An Intelligently Deformable Mirror For Space Telescope Technology," *J. Optical Engineering, V 33, N 3.*
4. Dainty, J. C., Koryabin, A.V., Kudryashov,A.V., , 1998,"Low-Order Adaptive Deformable Mirror," *J Applied Optics, V 37, N 21.*
5. Hoppmann, W.H.,II, Cohen, M.I., and Kunukkasseril, V.X., 1964, "Elastic Vibrations of Paraboloidal Shells of Revolution," *The Journal of the Acoustic Society of America*, Vol.36, No.2, pp.349-353.
6. Glockner, P.G. and Tawardros, K.Z., 1973, "Experiments on Free Vibration of Shells of Revolution," *Experimental Mechanics*, Vol.13, No.10, pp.411-421.
7. Shoemaker, W.L., and Utku, S., 1986, "On the Vibrations of Spinning Paraboloids," *Journal of Sound and Vibration*, Vol.111, No.2, pp.279-296.
8. Elliott, G.H., 1988, "The Evaluation of the Modal Density of Paraboloidal and Similar Shells," *Journal of Sound and Vibration*, Vol.126, No.3, pp.477-483.
9. Kayran, A., Vinson, J.R., and Ardic, E.S., 1994, "A Method for the Calculation of Natural Frequencies of Orthotropic Axisymmetrically Loaded Shells of Revolution," *ASME Transactions, Journal of Vibration & Acoustics*, Vol.116, pp.16-25.
10. Tzou, H.S., Zhong, J.P., and Hollkamp, J.J., 1994, "Spatially Distributed Orthogonal Piezoelectric Shell Actuators (Theory and Applications)," *Journal of Sound and Vibration,* Vol.177, No.3, pp.363-378.
11. Tzou, H.S., 1993, *Piezoelectric Shells: Distributed Sensing and Control of Continua*, Kluwer Academic Publishers, Boston/Dordrecht.
12. Tzou, H.S., Bao, Y., and Venkayya, V.B., 1996, "Parametric Study of Segmented Transducers Laminated on Cylindrical Shells, Part 2. Actuator Patches," *Journal of Sound and Vibration*, Vol. 197, No.2, pp.225-249.
13. Birman, V., Griffin, S., and Knowles, G., 2000, "Axisymmetric Dynamics of Composite Spherical Shells with Active Piezoelectric/Composite Stiffeners," *Acta Mechanica,* Vol.141, No.1, pp.71-83.
14. Zhou, Y.H. and Tzou, H.S., 2000, "Control of Nonlinear Piezoelectric Circular Shallow Spherical Shells," *Journal of Solids and Structures,* Vol.37, pp.1663-1677.
15. Tzou, H.S., Wang, D.W., and Chai, W.K., 2001, "Dynamics and Distributed Control of Conical Shells Laminated with Full and Diagonal Actuators," *Journal of Sound and Vibration.* (To appear)
16. Tzou, H.S. and Wang, D.W., 2002, "Distributed Signals of Piezoelectric Laminated Toroidal Shell Structures," *Journal of Sound and Vibration.* (To appear)
17. Tzou, H.S. and Ding, J.H., 2001, "Distributed Modal Signals of Nonlinear Paraboloidal Shells with Distributed Neurons," No.VIB21545, 2001 Design Technical Conference, Pittsburgh, PA, Sept.9-12, 2001.
18. Tzou, H.S., and Bao, Y., 1997, "Nonlinear Piezothermoelasticity and Multi-Field Actuations, Part 1: Nonlinear Anisotropic Piezothermoelastic Shell Laminates," *ASME Journal of Vibration and Acoustics*, Vol.119, pp.374-389.